Nano–bio interface between human plasma and niosomes with different formulations indicates protein corona patterns for nanoparticle cell targeting and uptake

Esther Imperlini,‡[a] Christian Celia,‡[b] Armando Cevenini,‡[c,d] Annalisa Mandola,[d,e] Maddalena Raia,[d] Massimo Fresta,[f] Stefania Orrù,*[d,e] Luisa Di Marzio,*[b] Francesco Salvatore*[c,d]

[a]IRCCS SDN, Napoli, Italy
[b]Dipartimento di Farmacia, Università di Chieti-Pescara "G. d'Annunzio", Chieti, Italy
[c]Dipartimento di Medicina Molecolare e Biotecnologie Mediche, Università degli Studi di Napoli "Federico II", Napoli, Italy
[d]CEINGE-Biotecnologie Avanzate S.c.a r.l., Napoli, Italy
[e]Dipartimento di Scienze Motorie e del Benessere, Università "Parthenope", Napoli, Italy
[f]Dipartimento di Scienze della Salute, Università "Magna Graecia" di Catanzaro, Campus Universitario "S. Venuta", Catanzaro, Italy

*Corresponding Authors: orru@uniparthenope.it; luisa.dimarzio@unich.it; salvator@unina.it

‡These authors contributed equally to this work.

Supplementary Results

Turbiscan Lab® Expert analysis of niosomes. The stability of NIOs was carried out using the Turbiscan Lab® Expert apparatus that measures without any invasive and destructive procedure the potential aggregation occurred for NIOs after their synthesis. The stability of NPs, and particularly NIOs, is an important requirement for PrC analysis *in vitro*, because fibrinogen that is a normal component of HP tends to be adsorbed on the surface of NPs and forms *in situ* aggregates which are not present *in vivo* due to the flowing effect of the blood stream. [1] In this scenario, aggregations might affect the average size of NPs and modify the composition and abundance of PrC.

We previously demonstrated that Turbiscan Lab® Expert can predict the stability of budenoside phosphate-loaded NIOs [2] as well as other colloidal formulations. [3-5]

The stability of NIOs was tested by measuring the optical transmission and the photon backscattering profiles of various formulations. In fact, variations of the vesicle volume fraction (migration) or mean size (coalescence) caused the variation of backscattering and transmission signals of NIOs, which were graphically reported as positive (backscattering/transmission increase) or negative (backscattering/transmission decrease) peaks. Data previously reported showed that any variation of particle size occurred when the ΔBS and ΔT profiles were in the range of variation between ±2% of the threshold line; while variations over ±10% indicated that NPs were unstable. [6]

The ΔBS profile of NIOs was stable and corresponded to the threshold baseline of measurements after 1 h of analysis (Figure S1). Results showed that the ΔBS signals were closed to ±0.5% during the time of analysis for the entire height of the samples; and positive or negative peaks were not present in the range of height between 2 mm and 13 mm (Figure S1). Positive and negative peaks below 2 mm depended on the air in the bottom and/or on the top of the cylindrical glass tube holding NIOs and were not related to aggregation or coalescence of samples during the analysis. These results are in agreement with those previously reported. [2] All the NIOs were stable and their stability was independent of the extrusion procedure and the composition (Figure S2). The transmission stability index (TSI) of NIOs supported the ΔBS data and demonstrated that all NIOs were stable during the analysis (Figure S2). In fact, TSI of NIOs were below 10 and any variation occurred during the analysis as previously reported for sclareol-loaded hyaluronan-coated PLGA nanoparticles. [7]

Supplementary References

(1). Hadjidemetriou, M.; McAdam, S.; Garner, G.; Thackeray, C.; Knight, D.; Smith, D.; Al-Ahmady, Z.; Mazza, M.; Rogan, J.; Clamp, A.; Kostarelos, K., The Human In Vivo Biomolecule Corona onto PEGylated Liposomes: A Proof-of-Concept Clinical Study. *Advanced Materials* **2019,** 31, (4).

(2). Marianecci, C.; Paolino, D.; Celia, C.; Fresta, M.; Carafa, M.; Alhaique, F., Non-ionic surfactant vesicles in pulmonary glucocorticoid delivery: Characterization and interaction with human lung fibroblasts. *Journal of Controlled Release* **2010,** 147, (1), 127-135.

(3). Di Francesco, M.; Primavera, R.; Fiorito, S.; Cristiano, M. C.; Taddeo, V. A.; Epifano, F.; Di Marzio, L.; Genovese, S.; Celia, C., Acronychiabaueri Analogue Derivative-Loaded Ultradeformable Vesicles: Physicochemical Characterization and Potential Applications. *Planta Medica* **2017,** 83, (5), 482-491.

(4). Cosco, D.; Paolino, D.; De Angelis, F.; Cilurzo, F.; Celia, C.; Di Marzio, L.; Russo, D.; Tsapis, N.; Fattal, E.; Fresta, M., Aqueous-core PEG-coated PLA nanocapsules for an efficient entrapment of water soluble anticancer drugs and a smart therapeutic response. *European Journal of Pharmaceutics and Biopharmaceutics* **2015,** 89, 30-39.

(5). Molinaro, R.; Evangelopoulos, M.; Hoffman, J. R.; Corbo, C.; Taraballi, F.; Martinez, J. O.; Hartman, K. A.; Cosco, D.; Costa, G.; Romeo, I.; Sherman, M.; Paolino, D.; Alcaro, S.; Tasciotti, E., Design and Development of Biomimetic Nanovesicles Using a Microfluidic Approach. *Advanced Materials* **2018,** 30, (15).

(6). Celia, C.; Trapasso, E.; Cosco, D.; Paolino, D.; Fresta, M., Turbiscan Lab (R) Expert analysis of the stability of ethosomes (R) and ultradeformable liposomes containing a bilayer fluidizing agent. *Colloids and Surfaces B-Biointerfaces* **2009,** 72, (1), 155-160.

(7). Cosco, D.; Mare, R.; Paolino, D.; Salvatici, M. C.; Cilurzo, F.; Fresta, M., Sclareol-loaded hyaluronan-coated PLGA nanoparticles: Physico-chemical properties and in vitro anticancer features. *International Journal of Biological Macromolecules* **2019,** 132, 550-557.

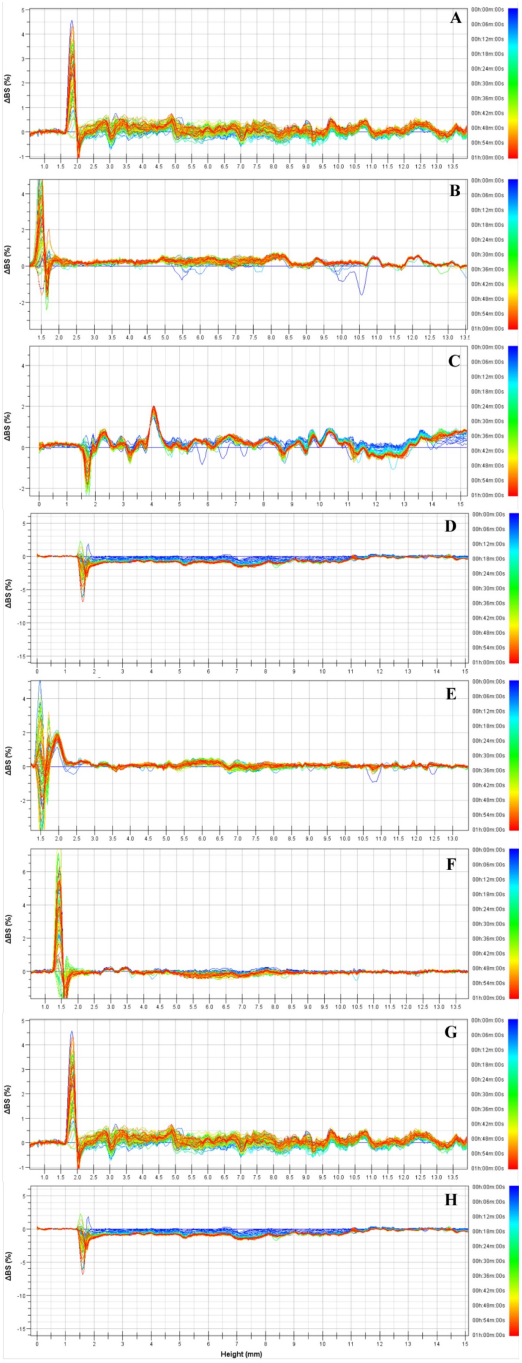

Supplementary Figure S1. Variation of backscattering (ΔBS) measurements of NIOs. ΔBS profiles of NIOs made up from different molar ratio of Tween® derivatives and cholesterol. (A) NIO1-200 and (B) NIO1-100 were made up from TW20:Chol (1:1 molar ratio); (C) NIO2-200 and (D) NIO2-100 were made up from TW80:Chol (1:1 molar ratio); (E) NIO3-200 and (F) NIO3-100 were made up from TW20:TW21:Chol (0.5:0.5:1 molar ratio); (G) NIO4-200 and (H) NIO4-100 were made up from TW80:TW21:Chol (0.5:0.5:1 molar ratio). Images are representative of triplicate experiments. The analysis was carried out using the Turbiscan Lab® Expert apparatus for 1 h at room temperature according to the procedure reported in the Materials and Methods section (see Turbiscan Lab Expert® analysis of niosomes).

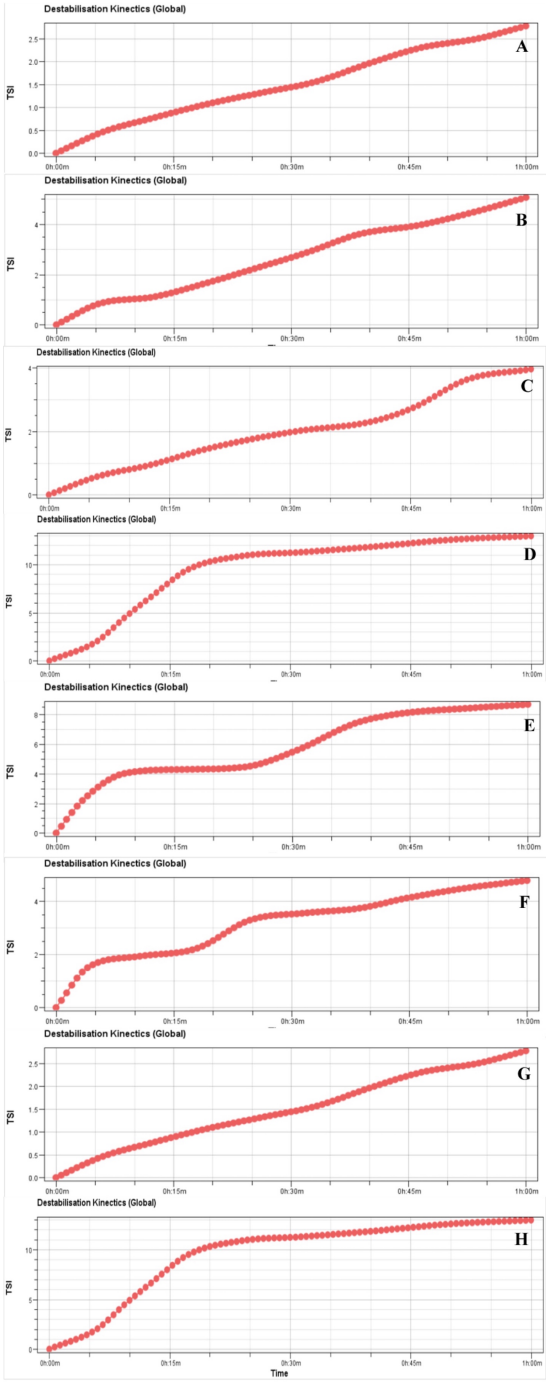

Supplementary Figure S2. Transmission stability index (TSI) measurements of NIOs. TSI measurements of NIOs made up from different molar ratio of Tween® derivatives and cholesterol. (A) NIO1-200 and (B) NIO1-100 were made up from TW20:Chol (1:1 molar ratio); (C) NIO2-200 and (D) NIO2-100 were made up from TW80:Chol (1:1 molar ratio); (E) NIO3-200 and (F) NIO3-100 were made up from TW20:TW21:Chol (0.5:0.5:1 molar ratio); (G) NIO4-200 and (H) NIO4-100 were made up from TW80:TW21:Chol (0.5:0.5:1 molar ratio). Images are representative of triplicate experiments. The analysis was carried out using the Turbiscan Lab® Expert apparatus for 1 h at room temperature according to the procedure reported in the Materials and Methods section (see Turbiscan Lab Expert® analysis of niosomes).

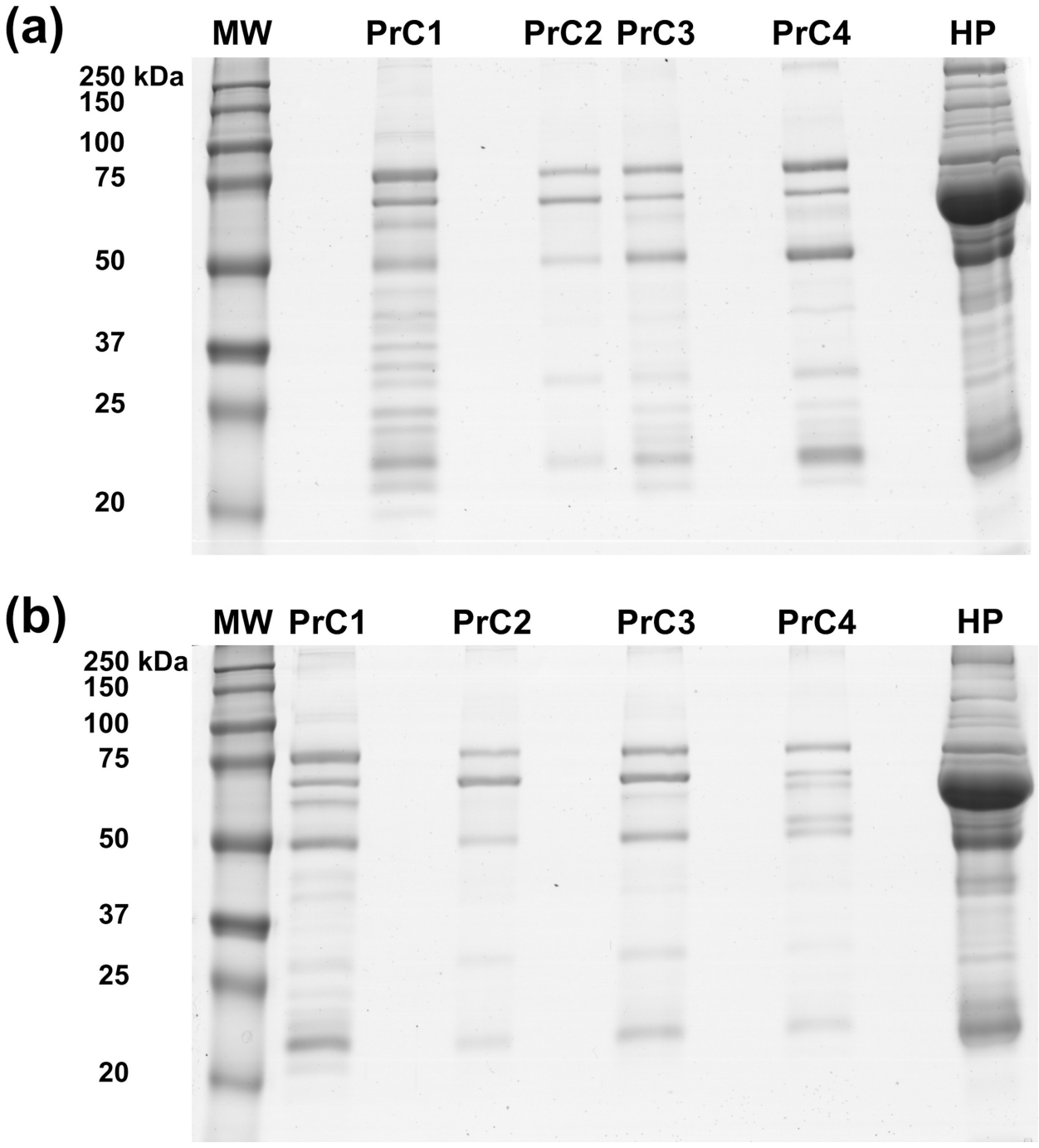

Supplementary Figure S3. SDS-PAGE analysis of PrC. Protein components were eluted from (a) NIO-100 and (b) NIO-200, and then separated by SDS-PAGE 12% (v/v). HP was loaded as a control. Protein bands were stained with Colloid Blue Stain Reagent and identified by LC–MS/MS analysis. PrC1/2/3 and 4: protein components adsorbed on NIO1/2/3 and 4, respectively.

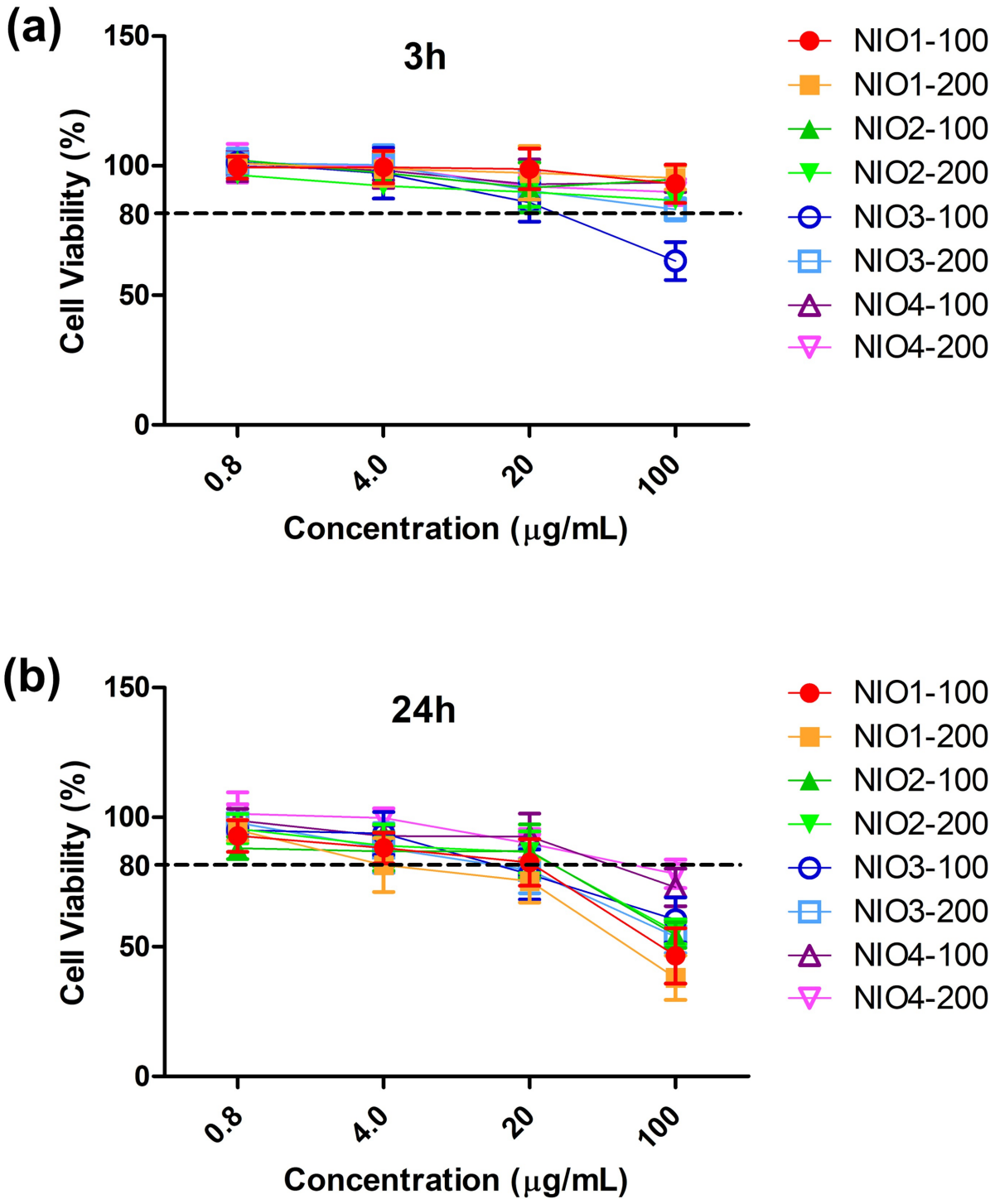

Supplementary Figure S4. Dependence of cell viability on NIO concentration. The viability of HCT-116 cells (a) at 3 h and (b) 24 h after treatment with different NIO concentrations was analyzed by MTT assay. Data were reported as percentages in comparison to the control (untreated cells). Error bars represent SD.

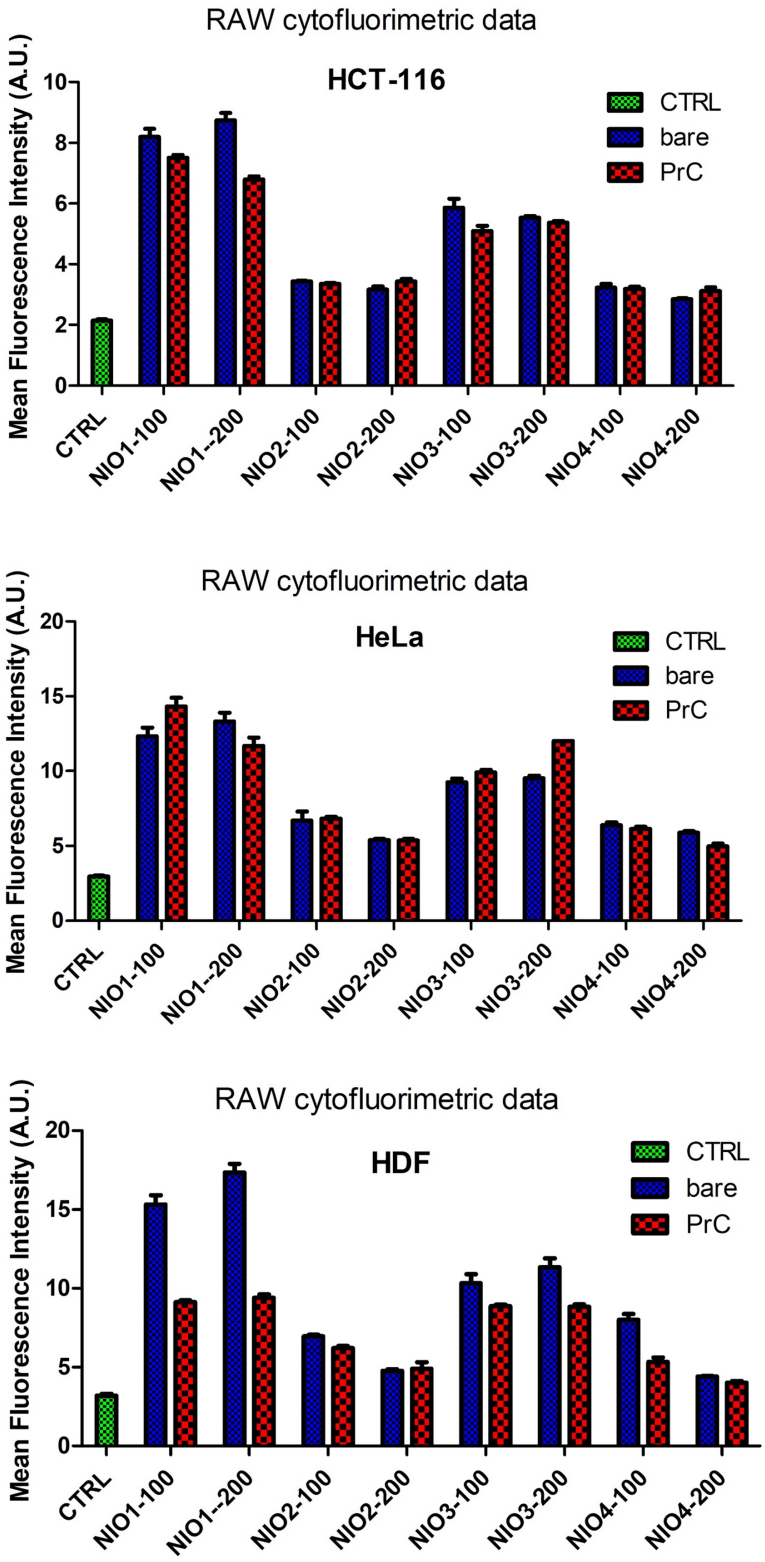

Supplementary Figure S5. Graphical report of cytofluorimetric raw data for the cellular uptake of fluorescent NIOs. The uptake was determined by flow cytometry on a Beckman Coulter FC500 measuring the mean fluorescence (MFI) of cells. Results are reported as mean values ±SD from three independent experiments.

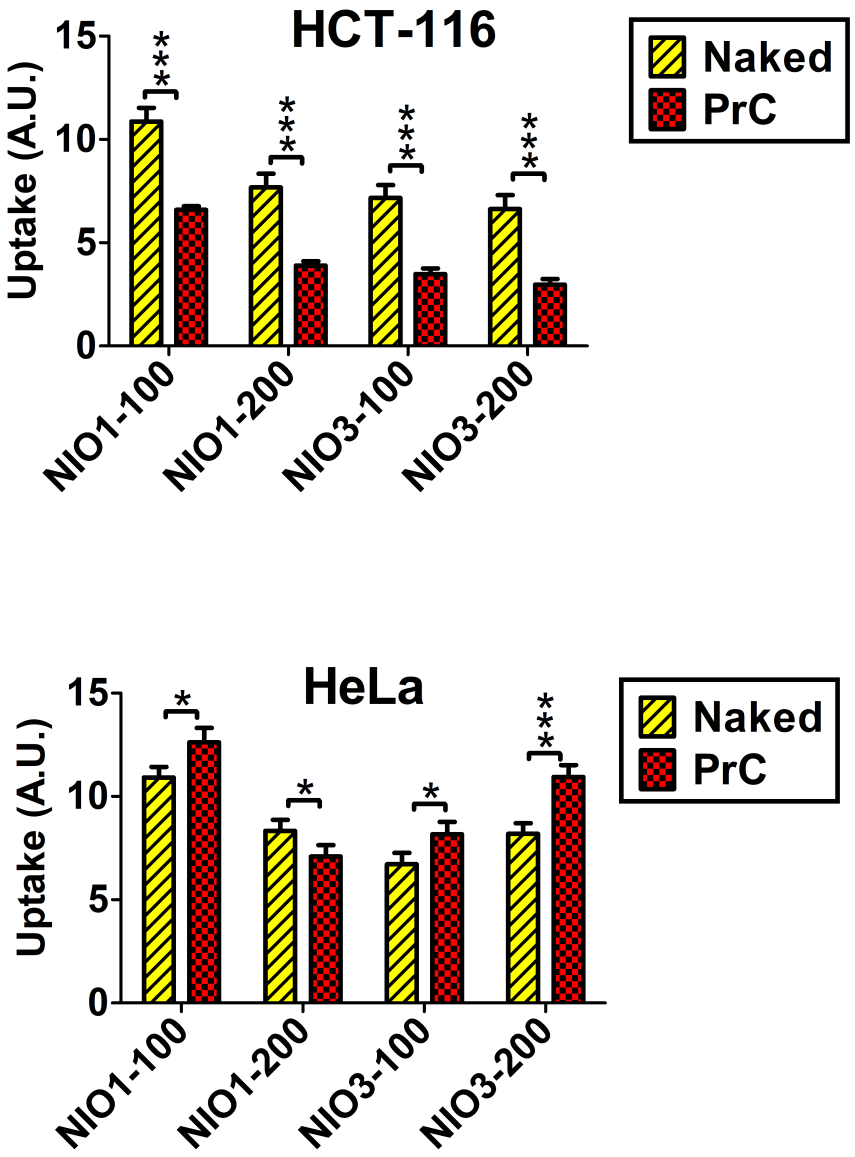

Supplementary Figure S6. Cellular uptake of naked NIOs and PrC-NIOs. HCT-116 and HeLa were incubated in: i) serum-free medium enriched in fluorescent naked NIO1 and NIO3 and ii) serum-free medium containing 1% HP enriched in fluorescent PrC-NIO1 and PrC-NIO3 (100 nm and 200 nm). Their uptake was quantified by flow cytometry measuring the mean fluorescence (MFI) of cells in three independent replicate experiments. Uptake levels are reported in graphs as the mean values ± SD and the statistical significance of pairwise comparison between naked and the corresponding coated NIO is showed, ** = $p < 0{,}01$; *** = $p < 0{,}005$.

Supplementary Table S1. Identification of protein corona (PrC) components for NIO1-100 and NIO1-200.

Uniprot	Protein	Gene	MW	Mascot Score (Peptide) 100nm	Mascot Score (Peptide) 200nm
P02549	Spectrin, alpha, erythrocytic 1	SPTA1	280699	888(16)	ND
P16157	Ankyrin-1 isoform 4	ANK1	204476	911(14)	184(3)
P12259	Coagulation factor V precursor	F5	252732	256(5)	611(10)
P11277	Spectrin beta chain, erythrocytic isoform b	SPTB	247171	1408(23)	166(3)
P01023	Alpha-2-macroglobulin precursor	A2M	164600	245(4)	ND
P07996	Thrombospondin-1 precursor	THBS1	133291	158(3)	526(9)
P02730	Band 3 anion transport protein	SLC4A1	102013	756(11)	490(7)
P00751	Chain B, structure of complement C3b: insights into complement activation and regulation	CFI	104912	219(4)	ND
P01871	Ig mu chain C region	IGHM	66596	6237(106)	5933(101)
P02768	Albumin	ALB	71246	1284(20)	1507(23)
P02787	Serotransferrin precursor	TF	79280	337(6)	164(3)
P04196	Histidine-rich glycoprotein precursor	HRG	60510	243(4)	196(3)
P04003	C4b-binding protein alpha chain precursor	C4BPA	69042	258(4)	186(3)
P01024	Chain A, Human Complement Component C3	C3	71317	117(2)	ND
P04004	Vitronectin	VTN	55165	127(2)	122(2)
P02790	Hemopexin precursor	HPX	52385	ND	98(2)
P01009	Alpha-1-antitrypsin	SERPINA1	44305	149(2)	198(3)
P02675	Chain B, crystal structure of human fibrinogen	FGB	52908	362(6)	ND
P01857	Ig G1 H Nie	IGHG1	49801	3671(64)	5086(91)
P02679	Fibrinogen gamma chain isoform gamma-A precursor	FGG	50092	136(2)	ND
P60709	Actin, cytoplasmic 1	ACTB	42052	184(3)	225(4)
O43866	CD5 antigen-like precursor	CD5L	39603	370(6)	593(9)
P00739	Haptoglobin-like protein	HPR	39496	321(5)	308(5)
Q9Y6Z7	Collectin 10	COLEC10	31113	105(2)	104(2)
P02649	Apolipoprotein E	APOE	36242	875(12)	966(14)
O75636	Ficolin-3 isoform 1 precursor	FCN3	33395	162(3)	300(5)
P02745	Complement C1q subcomponent subunit A precursor	C1QA	26285	162(3)	166(3)
P01834	Immunoglobulin kappa light chain VLJ region	IGK	28556	2135(37)	2311(39)
P02746	C1q B-chain precursor	C1QB	24154	258(4)	200(3)
P0CG04	Immunoglobulin lambda-chain	IGL	25172	210(4)	306(6)
P27105	Stomatin peptide	STOM	31860	356(5)	223(4)
P02647	Apolipoprotein A-I preproprotein	APOA1	30759	335(5)	253(4)
P02747	Complement C1q subcomponent subunit C precursor	C1QC	25985	190(3)	244(4)
P32119	Peroxiredoxin-2	PRDX2	22049	100(2)	ND

MW: molecular weight**;** ND: not determined**.**

Supplementary Table S2. Identification of protein corona (PrC) components for NIO2-100 and NIO2-200.

Uniprot	Protein	Gene	MW[a]	Mascot Score (Peptide) 100nm	Mascot Score (Peptide) 200nm
P15924	Desmoplakin I	DPI	334023	241(5)	ND
P02549	Spectrin, alpha, erythrocytic 1	SPTA1	280699	ND	382(7)
P12259	Coagulation factor V precursor	F5	252732	ND	344(6)
P11277	Beta-spectrin	SPTB	247026	148(2)	898(15)
P16157	Ankyrin-1 isoform 4	ANK1	204476	ND	547(9)
P01023	Alpha-2-macroglobulin precursor	A2M	164600	ND	118(2)
P07996	Thrombospondin-1 precursor	THBS1	133291	ND	224(4)
P02730	Band 3 anion transport protein	SLC4A1	102013	705(11)	847(13)
P02787	Serotransferrin precursor	TF	79280	553(8)	929(14)
P01024	Chain A, Human Complement Component C3	C3	71317	301(5)	437(7)
P02768	Albumin	ALB	71246	1524(23)	1466(22)
P11171	Protein 4.1 isoform 6	EPB41	66756	ND	163(3)
P01871	Ig mu chain C region	IGHM	66596	4030(70)	3568(60)
P04196	Histidine-rich glycoprotein precursor	HRG	60510	110(2)	124(2)
P04040	Catalase	CAT	59947	ND	255(4)
P04004	Vitronectin	VTN	55165	ND	186(3)
P02774	Serum vitamin D-binding protein precursor	GC	54612	ND	160(3)
P02675	Chain B, Crystal Structure Of Human Fibrinogen	FGB	52908	134(2)	272(5)
P02679	Fibrinogen gamma chain isoform gamma-A precursor	FGG	50092	ND	174(3)
P01011	Alpha1-antichymotrypsin, partial	SERPINA3	49986	ND	183(3)
P01857	Ig G1 H Nie	IGG	49801	2985(51)	3385(59)
P00738	Haptoglobin-like protein	HPR	45860	177(3)	193(3)
P01009	Alpha-1-Antitrypsin	SERPINA1	44305	1941(3)	265(4)
P60709	Actin, cytoplasmic 1	ACTB	42052	214(4)	321(6)
O43866	CD5 antigen-like precursor	CD5L	39603	341(5)	365(6)
P01876	Ig alpha-1 chain C region, partial	IGHA1	38486	367(6)	119(2)
P13716	delta-aminolevulinate dehydratase	ALAD	36758	110(2)	117(2)
P01859	Ig gamma-2 chain C region	IGHG2	36505	365(7)	1228(22)
P02649	Apolipoprotein E	APOE	36242	884(13)	993(14)
O75636	Ficolin-3 isoform 1 precursor	FCN3	33395	302(5)	244(4)
P27105	Stomatin peptide	STOM	31860	268(4)	203(3)
P02647	Apolipoprotein A-I preproprotein	APOA1	30759	291(4)	151(2)
P02747	Complement C1q subcomponent subunit C precursor	C1QC	25985	261(4)	190(3)
P02746	C1q B-chain precursor	C1QB	24154	181(3)	106(2)
P01834	Immunoglobulin kappa light chain VLJ region	IGK	28556	4478(74)	2921(45)
P32119	Peroxiredoxin-2	PRDX2	22049	ND	159(3)
P01591	Ig J-chain, partial	IGJ	16041	ND	162(3)
P47929	Galectin-7	LGALS7	15123	242(3)	ND
P02724	Glycophorin alpha	GYPA	14344	ND	137(2)

MW: molecular weight**;** ND: not determined**.**

Supplementary Table S3. Identification of protein corona (PrC) components for NIO3-100 and NIO3-200

Uniprot	Protein	Gene	MW	Mascot Score (Peptide) 100nm	Mascot Score (Peptide) 200nm
P15924	Desmoplakin I	DPI	334023	132(2)	ND
P02549	Spectrin, alpha, erythrocytic 1	SPTA1	280699	ND	600(10)
P11277	Spectrin beta chain, erythrocytic isoform b	SPTB	247171	ND	1237(20)
P16157	Ankyrin-1 isoform 4	ANK1	204476	ND	549(8)
P01023	Alpha-2-macroglobulin precursor	A2M	164600	ND	118(2)
P00450	Ceruloplasmin, partial	CP	116197	ND	102(2)
P02730	Band 3 anion transport protein	SLC4A1	102013	445(7)	748(11)
P0C0L4	Chain B, Human Complement C4	C4B	84758	ND	201(4)
P14923	Plakoglobin	JUP	82381	117(2)	ND
P02787	Serotransferrin precursor	TF	79280	226(4)	524(8)
P01024	Chain A, Human Complement Component C3	C3	71317	ND	516(7)
P02768	Albumin	ALB	71246	1286(20)	1484(23)
P01871	Ig mu chain C region	IGHM	66596	4412(75)	2608(43)
P04196	Histidine-rich glycoprotein precursor	HRG	60510	200(3)	ND
P04040	Catalase	CAT	59947	ND	154(2)
P04004	Vitronectin	VTN	55165	115(2)	171(3)
P02774	Serum vitamin D-binding protein precursor	GC	54612	ND	158(3)
P02675	Chain B, Crystal Structure Of Human Fibrinogen	FGB	52908	ND	393(6)
P02790	Hemopexin precursor	HPX	52385	ND	93(2)
P02679	Fibrinogen gamma chain isoform gamma-A precursor	FGG	50092	ND	202(4)
P01011	Alpha1-antichymotrypsin, partial	SERPINA3	49986	152(2)	129(2)
P01009	Alpha-1-Antitrypsin	SERPINA1	44305	187(3)	192(3)
O43866	CD5 antigen-like precursor	CD5L	39603	237(4)	260(4)
P00739	Haptoglobin-like protein	HPR	39496	115(2)	250(4)
P01859	Ig gamma-2 chain C region	IGHG2	36505	1288(22)	3303(57)
P02649	Apolipoprotein E	APOE	36242	921(14)	810(12)
P13716	Delta-aminolevulinate dehydratase	ALAD	36758	ND	111(2)
P04406	Glyceraldehyde-3-phosphate dehydrogenase	GAPDH	36202	ND	203(3)
O75636	Ficolin-3 isoform 1 precursor	FCN3	33395	261(4)	343(5)
P27105	Stomatin peptide	STOM	31860	117(2)	218(3)
P02647	Apolipoprotein A-I preproprotein	APOA1	30759	177(2)	255(3)
P0CG04	Immunoglobulin lambda light chain VLJ region	IGL	28305	574(11)	471(8)
P31944	Caspase-14 precursor	CASP14	27947	ND	218(3)
P02745	Complement C1q subcomponent subunit A precursor	C1QA	26285	102(2)	ND
P02747	Complement C1q subcomponent subunit C precursor	C1QC	25985	324(5)	243(4)
P02746	C1q B-chain precursor	C1QB	24154	248(4)	261(4)
P01834	Immunoglobulin kappa light chain VLJ region	IGK	22912	2237(35)	1370(23)
P32119	Peroxiredoxin-2	PRDX2	22049	ND	246(4)
P01591	Ig J-chain, partial	IGJ	16041	188(3)	ND
P47929	Galectin-7	LGALS7	15123	163(2)	ND
P02724	Glycophorin alpha	GYPA	14344	ND	143(2)

MW: molecular weight**;** ND: not determined**.**

Supplementary Table S4. Identification of protein corona (PrC) components for NIO4-100 and NIO4-200

Uniprot	Protein	Gene	MW	Mascot Score (Peptide) 100nm	Mascot Score (Peptide) 200nm
P02675	Chain B, Crystal Structure of Human Fibrinogen	FGB	52908	128 (2)	ND
P02768	Serum albumin	ALB	71246	1000(16)	1206(20)
P01871	Ig mu chain C region	IGHM	50123	355(6)	503(8)
O43866	CD5 antigen-like precursor	CD5L	39603	222(3)	169(3)
P01877	Immunoglobulin alpha-2 heavy chain	IGHA2	36526	226(4)	267(5)
P02649	Apolipoprotein E	APOE	36302	494(9)	290(5)
O75636	Ficolin-3 isoform 1 precursor	FCN3	33381	102(2)	ND
P01766	Immunoglobulin heavy chain variable region	IGHV3	12943	1016(18)	624(11)
P01834	Immunoglobulin kappa light chain VLJ region	IGK	11904	229(4)	233(4)

MW: molecular weight**;** ND: not determined**.**

Supplementary Table S5. The sizes of bare NIOs (Fig. 2a) were correlated with uptake levels of both bare NIOs and PrC-NIOs (Fig. 5) in HCT-116, HeLa and HDF cells.

	R[a]	
	bare NIOs	**PrC-NIOs**
HCT-116	**0.039**	**0.010**
HeLa	**-0.091**	**-0.040**
HDF	**-0.043**	**-0.062**

[a]R: the Pearson's correlation coefficient.